

**OPEN ACCESS**

## Electrochemical Analysis of an Electrolyte-Supported Solid Oxide Cell-Based MK35x Stack during Long-Term Electrolysis Operation

To cite this article: Matthias Riegraf *et al* 2024 *J. Electrochem. Soc.* **171** 054504

View the [article online](#) for updates and enhancements.

### You may also like

- [Confined Functionalization of Mesoporous Silicon Layers](#)  
Veronica Valentini and Riccardo Polini
- [Degradation Behavior of MK35x Stacks with Chromium-Based Interconnects in Steam Electrolysis Operation](#)  
Matthias Riegraf, Patric Szabo, Michael Lang *et al.*
- [Tailoring the Electrochemical Behavior of Multiwalled Carbon Nanotubes Through Argon and Hydrogen Ion Irradiation](#)  
Jeffrey A. Nichols, Hiroaki Saito, Mark Hoefer *et al.*

## Your Lab in a Box!

The PAT-Tester-i-16: All you need for Battery Material Testing.

- ✓ **All-in-One Solution with Integrated Temperature Chamber (10-80°C)!**  
No additional devices are required to measure at a stable ambient temperature.
- ✓ **Fully featured Multichannel Potentiostat / Galvanostat / EIS!**  
Up to sixteen independent battery test channels, no multiplexing.
- ✓ **Ideally suited for High-Precision Coulometry!**  
Measure with excellent accuracy and signal-to-noise ratio at the same time.
- ✓ **Small Footprint, Easy to Setup and Operate!**  
Cableless connection of 3-electrode battery test cells. Full multi-user, multi-device control via LAN.



Learn more on our product website:



Download the Data Sheet (PDF):



Or contact us directly:

☎ +49 40 79012-734

✉ sales@el-cell.com

🌐 www.el-cell.com



# Electrochemical Analysis of an Electrolyte-Supported Solid Oxide Cell-Based MK35x Stack during Long-Term Electrolysis Operation

Matthias Riegraf,<sup>1,z</sup> Patric Szabo,<sup>1</sup> Michael Lang,<sup>1</sup> Rémi Costa,<sup>1</sup> Stefan Rothe,<sup>2</sup> Stefan Megel,<sup>2</sup> and Mihails Kusnezoff<sup>2</sup>

<sup>1</sup>German Aerospace Centre (DLR), Institute of Engineering Thermodynamics, 70569 Stuttgart, Germany

<sup>2</sup>Fraunhofer Institute of Ceramic Technologies and Systems (IKTS), 01277 Dresden, Germany

The currently ongoing scale-up of high-temperature solid oxide electrolysis (SOEL) requires an understanding of the underlying dominant degradation mechanisms to enable continuous progress in increasing stack durability. In the present study, the degradation behavior of SOEL stacks of the type “MK35x” with chromium-iron-yttrium (CFY) interconnects and electrolyte-supported cells (ESC) developed at Fraunhofer IKTS was investigated. For this purpose, the initial electrochemical performance of a 10-cell stack was characterized in various operating conditions in both fuel cell and electrolysis mode. Degradation was evaluated during galvanostatic steady-state steam electrolysis operation for more than 3000 h at an oxygen side outlet temperature of 816 °C and a current density of  $-0.6 \text{ A cm}^{-2}$  and showed an average voltage evolution rate of  $-0.3\%/kh$  demonstrating high stability. Initial and final characterization at the part load operating point at  $-0.39 \text{ A cm}^{-2}$  and 800 °C led to the determination of a positive overall degradation rate of 0.4%/kh showing a considerable impact of the operating conditions on the degradation rate. By means of electrochemical impedance spectroscopy analysis it was shown that the stack’s ohmic resistance increased whereas the polarization resistance decreased most likely due to an enhancement in LSMM/ScSZ oxygen electrode performance.

© 2024 The Author(s). Published on behalf of The Electrochemical Society by IOP Publishing Limited. This is an open access article distributed under the terms of the Creative Commons Attribution 4.0 License (CC BY, <http://creativecommons.org/licenses/by/4.0/>), which permits unrestricted reuse of the work in any medium, provided the original work is properly cited. [DOI: 10.1149/1945-7111/ad417f]



Manuscript submitted January 8, 2024; revised manuscript received April 9, 2024. Published May 7, 2024. *This paper is part of the JES Focus Issue on SOFC XVIII: Advances in Solid Oxide Fuel Cell and Electrolysis Cell Technology.*

The decarbonization of hard-to-abate sectors with energy-intensive processes can in many cases occur by electrification via power-to-X concepts that use renewable energy, water and carbon dioxide to produce commodity chemicals or e-fuels with a low carbon footprint.<sup>1</sup> The development of efficient and cost-effective electrolysis technologies is key for the mass rollout of power-to-X projects. Among the different technologies, high-temperature solid oxide electrolysis (SOEL) offers by far the highest electrical efficiencies due to kinetic and thermodynamic advantages.<sup>2</sup>

Reliable long-term operation is a key factor for the wide-scale acceptance of SOEL, and therefore, significant development efforts are devoted to mitigating stack degradation. Degradation rates as low as 0.5% per 1000 h are targeted by the Strategic Research & Innovation Agenda from the Clean Hydrogen Joint Undertaking by 2030.<sup>3</sup>

While some in-depth degradation studies are available on cell level,<sup>4,5</sup> detailed investigations of SOEL stacks with operation for more than 1000 h are uncommon in literature.<sup>6–15</sup> Moreover, the stack degradation behavior is only rarely spatially resolved to the individual repeat units (RUs) by means of electrochemical impedance spectroscopy (EIS).<sup>7</sup>

The MK35x stack platform developed by IKTS is based on electrolyte supported cells (ESC) with chromium-iron-yttrium (CFY) interconnects.<sup>8,16–21</sup> The stacks were initially developed for SOFC operation where they showed an average voltage decrease of 0.7%/kh for more than 20,000 h and are commercially available.<sup>18</sup>

Here, the durability behavior of MK35x stacks tuned for operation in electrolysis mode is investigated in detail for more than 3000 h in order to obtain an in-depth understanding of the voltage evolution over time of the individual repeat units in the stack.

## Experimental

A 10-cell stack of the Mk35x design with metallic CFY ( $\sim 94 \text{ mol} \% \text{ Cr}$ ,  $5 \text{ mol} \% \text{ Fe}$ ,  $\sim 1 \text{ mol} \% \text{ Y}_2\text{O}_3$ ) interconnects developed by IKTS was operated in steam electrolysis.<sup>8,16,17,19,21</sup> The stack was

manufactured at the IKTS pilot line and had a cross flow design with internal fuel gas and open-air manifolds. Figure 1 shows the exploded view of the stack components and their assembly. The CFY interconnects had a size of  $13.0 \times 15.0 \text{ cm}^2$  and the electrolyte supported cells an active area of  $11.0 \times 11.5 \text{ cm}^2$  ( $127 \text{ cm}^2$ ). The ESCs use 10 mol%  $\text{Sc}_2\text{O}_3$ –1 mol%  $\text{CeO}_2$ –89 mol%  $\text{ZrO}_2$  (10Sc1CeSZ) electrolytes and are based on  $\text{La}_{1-x}\text{Sr}_x\text{Mn}_{1-y}\text{M}'_y\text{O}_{3-\delta}$  (LSMM', with M' being a transition metal)/ $\text{Sc}_2\text{O}_3$  stabilized  $\text{ZrO}_2$  (ScSZ) oxygen and Ni/Gadolinium-doped ceria (CGO) electrodes (type “IKTS-G5b”) optimized for electrolysis operation.<sup>22</sup> After a quality check of every component and assembly, the stack was sealed, joined (for high-temperature glass to metal bonding), initialized (NiO reduced to metallic Ni) and pre-tested at IKTS.<sup>21</sup> Then the 10-cell stack was dispatched for integration and operated in a test rig at DLR with controlled air and gas preheaters.

The 10 repeat units were numbered upwards from the bottom. The temperatures inside the external air manifolds at the inlet and outlet as well as the temperatures at three different positions inside the stack ( $T_4$  in RU 4,  $T_6$  in RU 6,  $T_{10}$  in RU 10) were monitored. All three thermocouples were inserted into the air channels until the middle of the stack. If not stated otherwise, the oxygen side outlet temperature inside the manifold is referred to as stack temperature. All gas constituents were supplied by mass flow controllers.

After heating up with  $2 \text{ K min}^{-1}$ , the gas-tightness of the different RUs was checked at an air outlet temperature of 770 °C with a fuel gas mixture of 40%  $\text{H}_2$ /60%  $\text{N}_2$ . A total air flow of  $20 \text{ L min}^{-1}$  (SLPM) was used for all tests. Then, an initial performance characterization was carried out by means of EIS at three operating points, the nominal full load operating point in fuel cell and the nominal full and part load operating points in electrolysis mode. In SOFC operation, a feed gas consisting of 40%  $\text{H}_2$ , 60%  $\text{N}_2$  and with a total flow rate of 8 SLPM was used and a current density of  $0.275 \text{ A cm}^{-2}$  was applied. In SOEL, the stack was first characterized at part load at a current density of  $-0.39 \text{ A cm}^{-2}$  with a total fuel gas flow rate of 5.4 SLPM (steam conversion (SC) of 82%). The oven temperature was adjusted for the oxygen side outlet temperature to reach 800 °C. Subsequently, the stack was characterized at the nominal full load operating point before starting a steam electrolysis long-term test. The inlet fuel gas

<sup>z</sup>E-mail: [Matthias.Riegraf@dlr.de](mailto:Matthias.Riegraf@dlr.de)

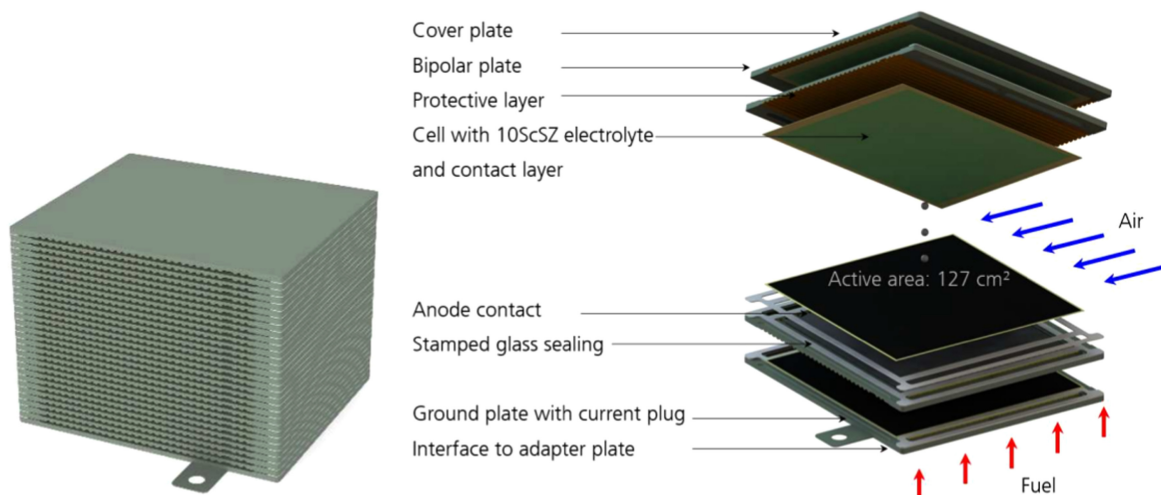


**Figure 1.** Illustration of a MK35x stack. 30-cell stack (left) and its exploded view (right).<sup>7</sup>

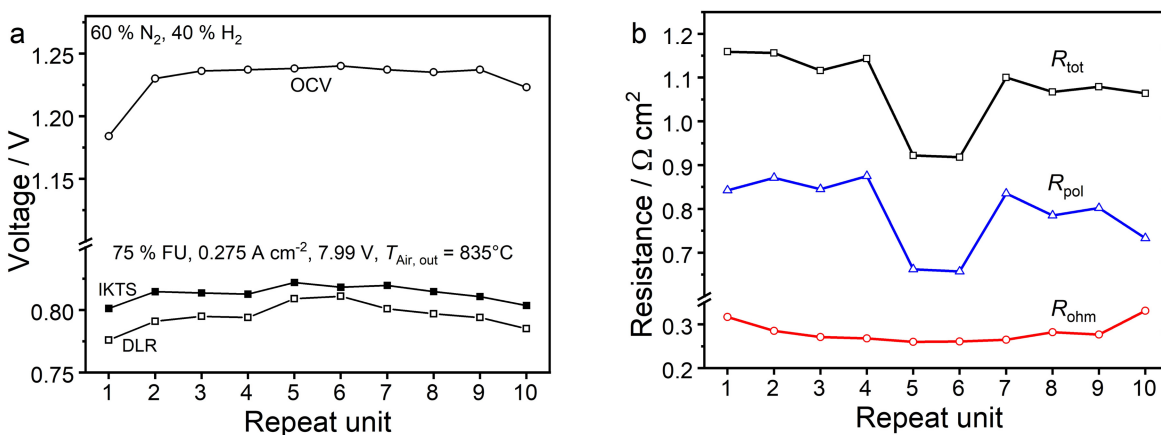


**Figure 2.** Diagrams depicting (a) voltage and (b) resistance homogeneity of the RUs inside the stack in SOFC operation with a fuel gas consisting of 60% N<sub>2</sub>, 40% H<sub>2</sub>. Voltage values are shown at OCV and at 0.275 A cm<sup>-2</sup> (75% FU). Reference values obtained at IKTS are inserted for comparison.

composition was 80% H<sub>2</sub>O and 20% H<sub>2</sub>, with a total fuel gas flow rate of 8.2 SLPM and a current density of  $-0.6 \text{ A cm}^{-2}$  was used leading to a SC of 82%. At the beginning of the durability test the oven temperature was set to the one used during fuel cell referencing which led to a stack temperature of 816 °C and was afterwards held constant during the following durability test.

Before cooling down, a final characterization of the stack's performance was carried out at different rated power. For this final characterization, the stack was electrochemically analyzed at the same reference points as at the start of operation with the initially set oven temperatures.

EIS measurements were carried out with an electrochemical workstation IM6 connected to an electronic load EL1000 (Zahner-Elektrik GmbH & CO. KG, Kronach, Germany). A voltage supply was integrated in the current circuit for SOEL measurements. An AC amplitude of  $15 \text{ mA cm}^{-2}$  with a frequency range of 20 mHz to 20 kHz was applied to the stack. The electrical current probes were connected to the top and bottom plates, while the voltage probes were attached at each repeat unit of the stack enabling EIS measurements at all single repeat units. Distribution of relaxation times (DRT) analysis was performed by using the modelling software ec-idea. A regularization parameter of 0.5 was chosen since it led to a small difference between the reconstructed and measured impedance spectra while avoiding over-regularization.<sup>23</sup> The fit of measured spectra with an equivalent circuit model (ECM) was carried out with the software ZView.

## Results and Discussion

### Electrochemical characterization in fuel cell operation.—

Electrochemical characterization of the stack in fuel cell operation was performed at the beginning of the test. Diagrams comprising the homogeneity of the voltages of the single RUs at open circuit voltage (OCV) and at 0.275 A cm<sup>-2</sup>, as well as their calculated ohmic, polarization and total resistance values are shown in Figs. 2a, 2b. Additionally, the reference voltage values obtained during the commissioning procedure at IKTS are depicted for comparison. In its initial state, at DLR the stack reached 0.28 kW with an electrical efficiency of 53.4%.

All OCV values except RU 1 were above 1.2 V confirming a generally good gas-tightness of the utilized setup and the stack. The OCV of the first RU was slightly below 1.2 V indicating a small leakage at the interface between the bottom plate of the stack and the external gas manifold plate.

The voltage values of RUs at 0.275 A cm<sup>-2</sup> (75% FU) at DLR ranged between 0.778 V and 0.810 V, and their distribution over the stack height was in good agreement with the values obtained during the commissioning test at IKTS. The difference between the voltage values for the different RUs measured at DLR and IKTS was in the range of 8–25 mV. The observed deviation was most likely due to a lower temperature of the air preheater at DLR test bench resulting in slightly lower average RU temperatures. Area-specific resistance (ASR) values were derived from the impedance spectra depicted in Fig. 3 and were between  $0.918 \text{ } \Omega \text{ cm}^2$  and  $1.157 \text{ } \Omega \text{ cm}^2$ . The

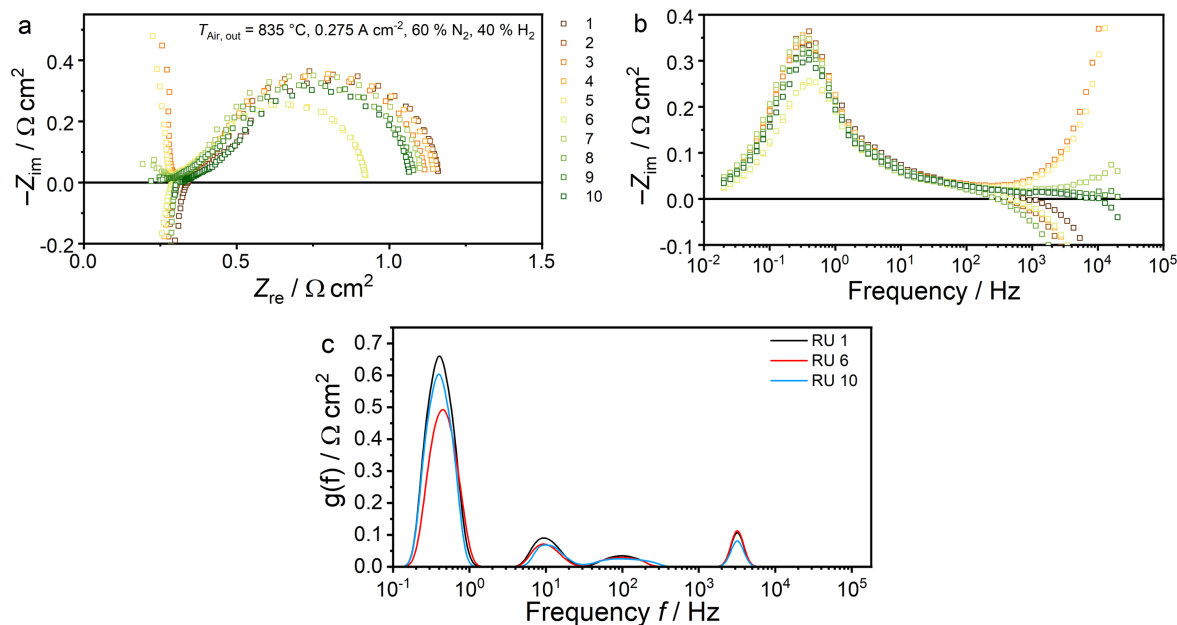


**Figure 3.** (a) Nyquist plot and (b) imaginary impedance plots of all EIS measurements, and (c) DRT analysis of EIS measurements for RU 1, 6 and 10 in SOFC operation with a fuel gas consisting of 60%  $\text{N}_2$ , 40%  $\text{H}_2$  at  $0.275 \text{ A cm}^{-2}$ . The numbers in the legend on the right side of (a) indicate the number of the respective RU.

distribution of both the ASR and the voltage over the height of the stack showed good agreement with a lower performance at the bottom and top RUs and slightly higher performance of the RUs in the middle of the stack. This is particularly evident for the ohmic resistance values shown in Fig. 2b with RU 5 and RU 6 showing the lowest values of  $0.26 \Omega \text{ cm}^2$  and RU 10 showing the highest value of  $0.33 \Omega \text{ cm}^2$ . At this operating point, temperatures of  $845 \text{ }^\circ\text{C}$  in RU 6 and  $837 \text{ }^\circ\text{C}$  in RU 10 were measured showing a non-uniform temperature distribution inside the stack during fuel cell operation, which is caused by the so-called “edge effect.”<sup>24</sup> During operation, the heat losses from the outer RUs to the top or bottom plate of the stack are higher compared to the RUs in the middle which have lower heat transfer to their adjacent RUs. Thus, higher temperatures occur in the middle cells, leading to lower ohmic and electrode resistances and better performance. However, the maximum relative increase of the ohmic resistance of the different repeat units of  $\sim 27\%$  is too high to be purely explained by the measured temperature difference within the stack. Thus, it is likely that deviations in contacting also contribute to the increased ohmic resistance values at the outer RUs.

However, the main reason for the significantly lower ASR of RU 5 and RU 6 in Fig. 2 is their low polarization resistance at frequencies  $\sim 0.5 \text{ Hz}$  (see Fig. 3). The imaginary parts of all spectra show a more similar behavior at higher frequencies until  $200 \text{ Hz}$ . At even higher frequencies, inductance phenomena are visible that differ between the different RUs most likely due to the different positions of the Pt wires used for voltage sensing that were welded to the interconnects. For further analysis of the loss contributions in the impedance spectra, a DRT analysis of selected RUs was performed (see Fig. 3c). At least four peaks could be observed at frequencies of  $\sim 5 \cdot 10^3 \text{ Hz}$ ,  $\sim 10^2 \text{ Hz}$ ,  $\sim 10 \text{ Hz}$  and  $\sim 0.5 \text{ Hz}$ . In previous work, the Ni/CGO surface exchange contribution of a G3 cell from IKTS was identified at frequencies of  $\sim 5 \text{ Hz}$  in SOFC operation.<sup>25</sup> Additionally, the main LSMM/ScSZ oxygen electrode contribution was observed at similar frequencies causing the two electrode peaks to overlap. The results in this work confirm the existence of the LSMM/ScSZ oxygen electrode process in this frequency range due to the activation of polarization resistance typical for LSM-based cathodes as seen in the following. The DRT peaks identified at higher frequencies could then be related to the Ni/CGO bulk process,

and interface processes.<sup>26–28</sup> The gas conversion impedance is often reported at low frequencies of  $\sim 0.5 \text{ Hz}$ ,<sup>7</sup> and becomes large when either steam or hydrogen partial pressures are low. At very low steam content at the inlet the gas conversion impedance dominates the total ASR. The gas conversion impedance generally slightly increases with increasing operating temperature.<sup>29</sup> Hence, in case of a homogeneous flow distribution the middle planes of stack should show slightly higher gas conversion losses. The gas conversion resistance variation between the different cells, which is correlated with gas flow distribution between the RUs in the stack, is the most likely explanation for the observed differences in polarization resistance. Analysis of the low frequency response of the impedance spectra shows that gas supply to RU 5, 6 and to a lower extent to RU 10 is higher in comparison to other planes (see Fig. 3). The imposition of an alternating current signal of  $0.015 \text{ A cm}^{-2}$  during the impedance measurements added a maximum fuel consumption of 4.1% to the base consumption of 75%. Therefore, it is possible that at such high fuel utilization values, the differences in gas flow distribution were even more apparent during the EIS measurements.

#### Electrochemical characterization in electrolysis operation.—

After initial characterization in SOFC operation, the stack was electrochemically characterized in SOEL. Figure 4 shows a diagram of the voltage homogeneity of the different RUs at two operating points at nominal full and part load. At both operating points with gas inlet mixtures  $80\% \text{ H}_2\text{O} + 20\% \text{ H}_2$  the steam conversion was kept constant at 82%. Only the current densities ( $-0.39$ ,  $-0.6 \text{ A cm}^{-2}$ ) and corresponding gas flow rates were different. Figure 4a shows the voltage homogeneity diagram before the subsequent durability test of  $-0.6 \text{ A cm}^{-2}$  with a stack temperature of  $816 \text{ }^\circ\text{C}$  and Fig. 4b the similar diagram at part load at a current density of  $-0.39 \text{ A cm}^{-2}$  and stack temperature of  $800 \text{ }^\circ\text{C}$ . In its initial state, the stack reached  $1.03 \text{ kW}$  with an electrical efficiency of 92.9% at the nominal operating point (slightly exothermal operation) with  $-0.6 \text{ A cm}^{-2}$ .

The OCV values of the RUs in both cases were very homogeneous with a maximum deviation of  $5 \text{ mV}$ , with RU 1 again showing the lowest value consistent with Fig. 1 confirming a small gas leakage. Nevertheless, the maximum temperature difference within the stack at OCV was below  $1 \text{ K}$  indicating no signs of large-scale burning. The

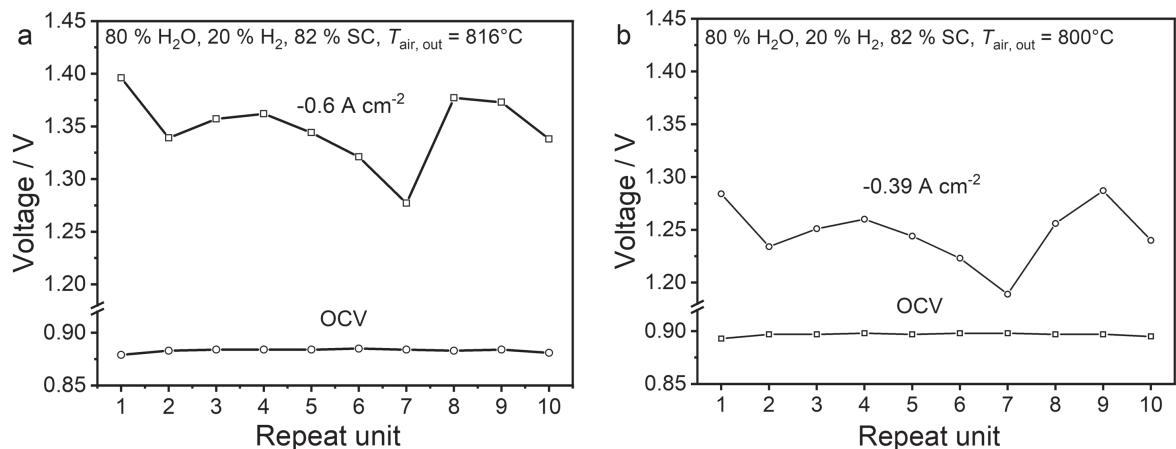


**Figure 4.** Voltage homogeneity diagram depicting voltage of the RUs inside the stack in SOEL with a gas consisting of 80% H<sub>2</sub>O and 20% H<sub>2</sub>. Voltage values are shown at OCV and at (a)  $-0.6 \text{ A cm}^{-2}$  and (b)  $-0.39 \text{ A cm}^{-2}$ .

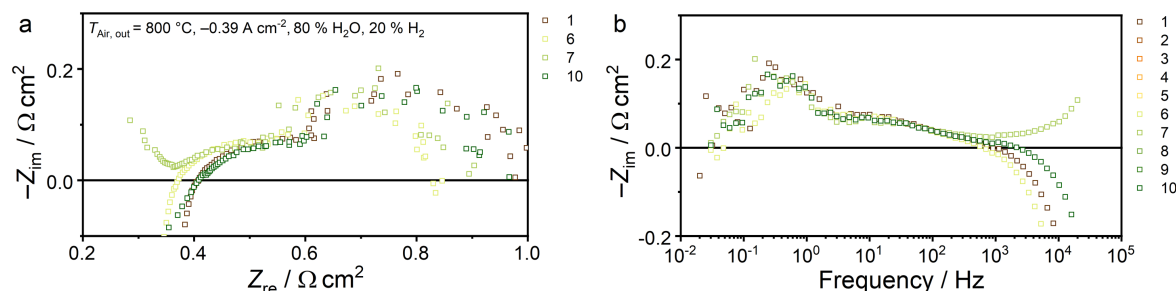


**Figure 5.** (a) Nyquist plot, (b) imaginary impedance plot of selected EIS measurements in SOEL with a fuel gas consisting of 80% H<sub>2</sub>O, 20% H<sub>2</sub> at  $-0.39 \text{ A cm}^{-2}$ . The numbers in the legend on the right side of the diagrams indicate the number of the respective RU.

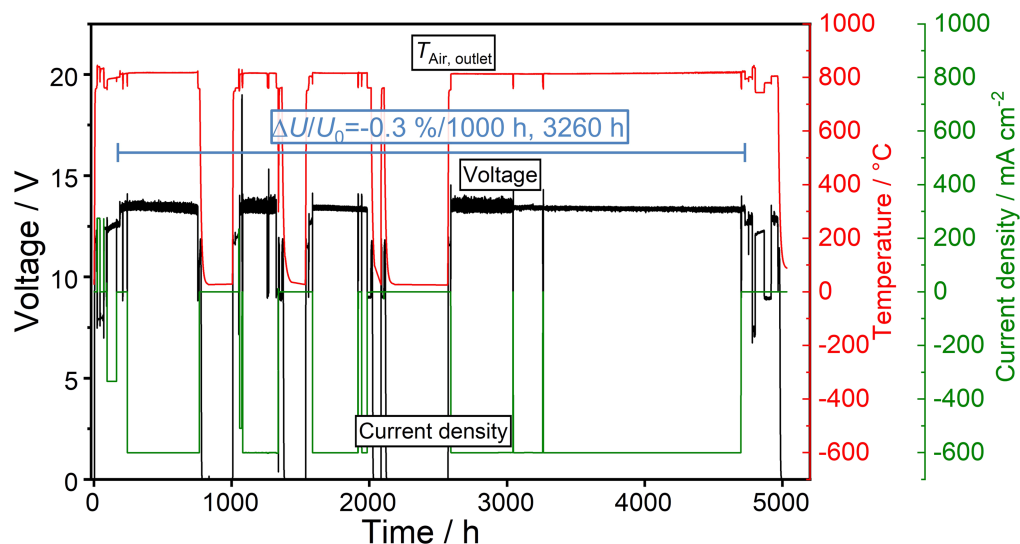


**Figure 6.** Long-term test of the stack at  $-0.6 \text{ A cm}^{-2}$  (82% SC) with gas composition 80% H<sub>2</sub>O and 20% H<sub>2</sub> on steam side and air as oxidant.

voltage values of all 10 RUs at  $-0.6 \text{ A cm}^{-2}$  and  $-0.39 \text{ A cm}^{-2}$  were within a range of 118 mV and 98 mV, respectively. The voltage homogeneity diagram in both cases showed a similar behavior over the height of the stack with the lowest voltage in RU 7, and local maxima at RU 1, RU 4 and RU 8 or RU 9. However, no clear edge effect was observed indicating the low temperature gradient over the height of the stack which is in good agreement with both average voltages being only slightly above ( $-0.6 \text{ A cm}^{-2}$ ) or below ( $-0.39 \text{ A cm}^{-2}$ ) the thermoneutral voltage. Therefore, most likely the voltage profiles in Fig. 4 follow the deviations in manufacturing-

related ASR differences of the different RUs. However, additional impedance spectra at OCV would be necessary to clarify this hypothesis to avoid any performance differences caused by a temperature profile due to heating or cooling inside the stack.

For further analysis, impedance spectra of selected RUs at  $-0.39 \text{ A cm}^{-2}$  are displayed in Fig. 5. RU 7 shows the lowest ohmic resistance among all cells, which is most likely the reason for its better performance. Considerable scattering of the impedance data in the low-frequency region impeded an exact determination of the polarization resistance.

**Table I.** Overview of the voltage evolution and degradation rates during the four periods of operation at the nominal operating point of  $-0.6 \text{ A cm}^{-2}$  and at the part load operating point with a current density of  $-0.39 \text{ A cm}^{-2}$ . Increase of average ASR value was calculated according to  $\Delta ASR = \Delta U / i/10$ .

	$-0.6 \text{ A cm}^{-2}$					$-0.39 \text{ A cm}^{-2}$ Total
	Phase 1	Phase 2	Phase 3	Phase 4	Total	
Beginning [h]	244	1084	1595	2599	244	200
End [h]	751	1321	1983	4728	4728	4942
Length [h]	507	237	388	2128	3260	3954 (used for normalization)
Initial voltage [V]	13.465	13.381	13.367	13.462	13.465	12.567
End voltage [V]	13.266	13.455	13.277	13.317	13.317	12.789
Absolute voltage change [mV]	-199	64	-90	-145	-148	222
Degradation rate [mV/kh]	-392	270	-232	-68	-45	56
Relative degradation [%]	-1.48	0.48	-0.67	-1.08	-1.1	1.7
Relative degradation rate [%/kh]	-2.92	2.02	-1.74	-0.51	-0.33	0.4
Average ASR increase per RU [ $\text{m}\Omega \text{ cm}^2/\text{kh}$ ]	65.3	45	-38.7	-11.3	-7.5	14.4

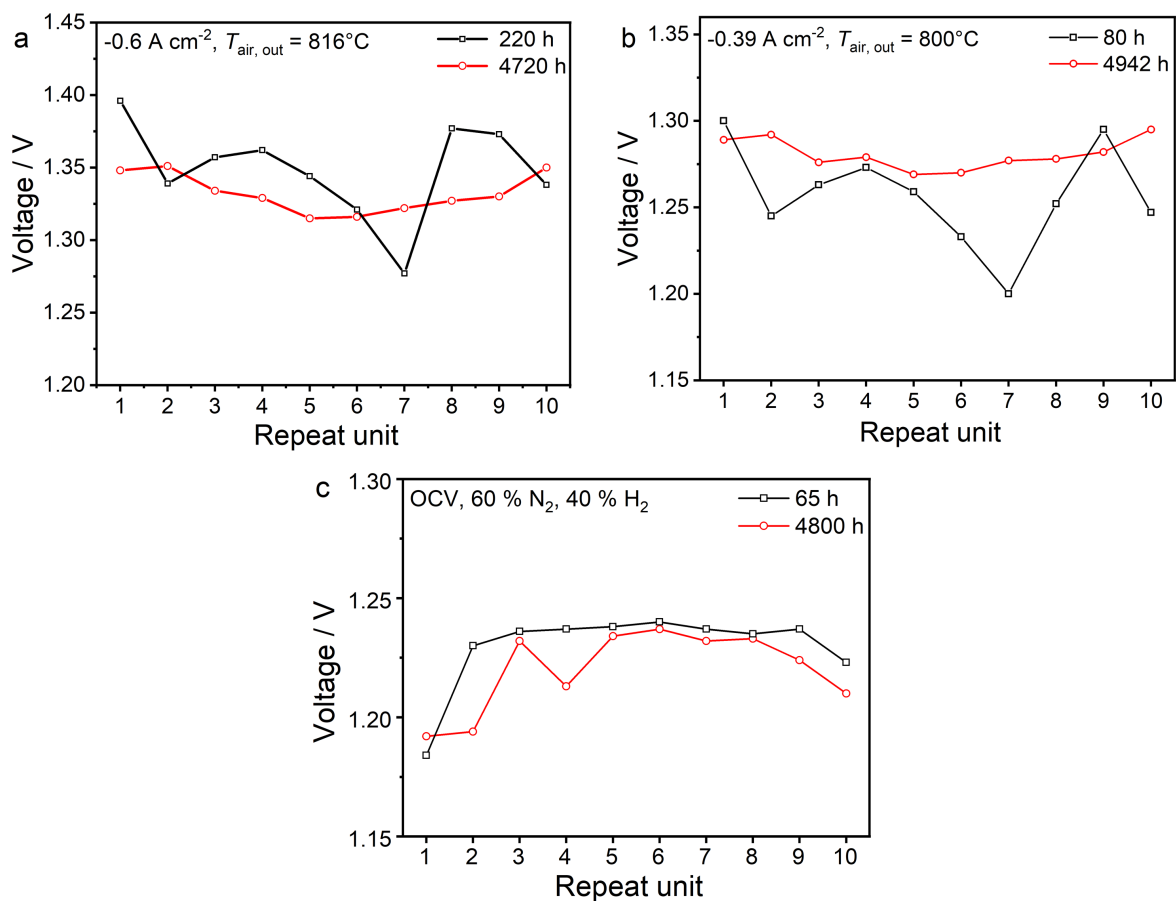


**Figure 7.** Homogeneity diagrams depicting the voltages of the RUs over time inside the stack (a) in SOEL at  $-0.6 \text{ A cm}^{-2}$  and (b) in SOEL at  $-0.39 \text{ A cm}^{-2}$  and (c) at SOFC conditions (60%  $\text{H}_2$ , 40%  $\text{N}_2$ ) at OCV with a temperature inside the stack of  $T = 787^\circ\text{C}$ .

However, compared to the EIS measurements in SOFC operation in Fig. 3, qualitatively only small deviations of the polarization resistance were observed. This difference in behavior is caused by a far lower contribution of the gas conversion impedance to the total ASR at higher steam content in the gas mixture (it is highest for a dry  $\text{H}_2/\text{N}_2$  mixture).<sup>29</sup> Nevertheless, RU 6 also seems to have the lowest gas conversion resistance in Fig. 6 confirming the increased gas supply hypothesized based on Fig. 3 above (the same holds true for RU 5 which is not shown here to improve diagram visibility).

**Long-term stability in electrolysis operation.**—After initial stack characterization, a SOEL durability test was performed at  $-0.6 \text{ A cm}^{-2}$ , which corresponds to 82% SC at a stack temperature of  $816^\circ\text{C}$ . The entire long-term behavior of the stack is depicted in Fig. 6. The test was performed over  $\sim 5000 \text{ h}$  during which the stack was operated for 3260 h at the nominal operating conditions. Significant voltage oscillations occurred especially in the first half of the test due to instabilities in the steam supply. This problem was resolved later by optimized operation of the humidifier. The operating time was subdivided into four periods (see Table I)

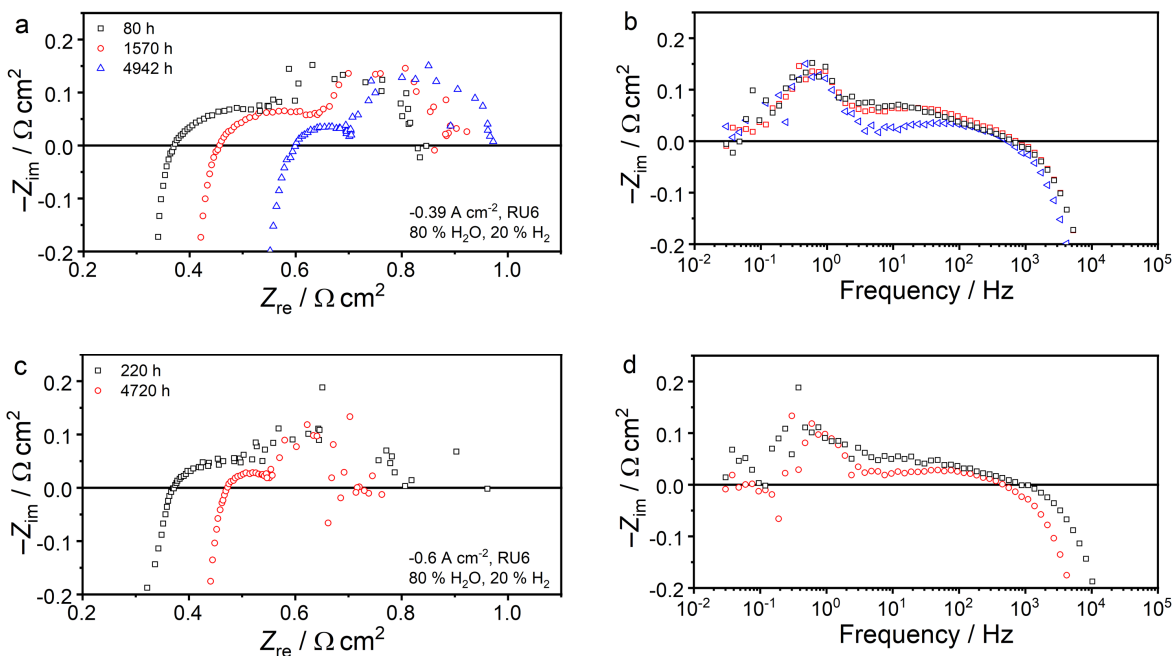


**Figure 8.** (a) Nyquist plot, (b) imaginary impedance plot of representative EIS spectra of RU 6 in electrolysis operation with gas composition consisting of 80% H<sub>2</sub>O and 20% H<sub>2</sub> at  $-0.39 \text{ A cm}^{-2}$ .  $T_{\text{air,out}}$  was 800 °C at 80 h, 802 °C after 1570 h and 805 °C after 4942 h. (c) Nyquist plot, (d) imaginary impedance plot of EIS spectra of RU 6 in electrolysis operation with gas composition consisting of 80% H<sub>2</sub>O and 20% H<sub>2</sub> at  $-0.6 \text{ A cm}^{-2}$ .  $T_{\text{air,out}}$  stayed constant at 816 °C for both measurements.

between which the test rig had to be cooled down for technical maintenance. Table I summarizes the degradation rates during all four periods and for the entire durability test.

Table I shows a decrease of the stack voltage in the operating phases 1, 3 and 4 leading to negative voltage degradation rates, which means an improvement of the performances in these time periods. During phase 2, a small degradation of 74 mV was observed. Over the course of the whole 3260 h at the nominal operating point including the thermal cycles, a decrease of the electrolysis voltage of  $-45 \text{ mV kh}^{-1}$  was observed which corresponds to a negative voltage degradation rate of  $-0.33\%/kh$  (performance enhancement) and demonstrates the outstanding stability of the MK35x stack in SOEL. The outlet temperature at the oxygen side showed a decrease of below 0.5 K over the course of the experiment at the nominal operating conditions with the oven temperature kept constant, confirming that due to the largely unaltered operating voltage no major change in stack temperature was observed.

For an in-depth understanding of the degradation behavior of the different RUs, their voltage degradation over time at the nominal operating point is summarized in Fig. 7a. In between  $t = 220 \text{ h}$  and  $t = 4720 \text{ h}$ , the voltage of nearly all RUs decreased considerably. RU 8 displayed the largest voltage decrease of 50 mV ( $-1.0\%/kh$ , normalized by 3594 h corresponding to the difference between the EIS measurements subtracted by time at room temperature). RU 2 and RU 10 showed a small increase in voltage by 12 mV respectively, whereas RU 7 was the only cell that displayed a significant voltage degradation of 55 mV ( $1.0\%/kh$ , normalized by 3592 h).

Furthermore, the change of the voltages of all RUs was also monitored at part load at  $-0.39 \text{ A cm}^{-2}$  at initial  $T_{\text{air,out}} = 800 \text{ °C}$ . The voltages during initial and final EIS characterization are depicted in Fig. 7b. In contrast to the results of Fig. 7a, except for RU 9 all RUs showed significant voltage degradation over time. Thus, interestingly, the degradation behavior of the stack strongly depends on the current density and the temperature of the EIS measurements, which can be explained as follows. At the part load operating point with  $i = 0.39 \text{ A cm}^{-2}$ , the stack voltage increased from 12.567 V after 200 h to 12.789 V after 4942 h during the

recording of the impedance spectra. This increase corresponds to an overall degradation of 222 mV and 1.7%, which amounts to a degradation rate of 0.4%/kh or an average  $14.4 \text{ m}\Omega \text{ cm}^2 \text{ kh}^{-1}$  per RU when normalized to the time period of 3954 h which corresponds to the time difference between the EIS measurements subtracted by the time at room temperature during the thermal cycles. Even at this operating point, the determined degradation rate matches the 0.5%/kh targeted by the Strategic Research & Innovation Agenda from the Clean Hydrogen Joint Undertaking by 2030,<sup>3</sup> and is in the range of the lowest values found in literature.<sup>6–8,11,12</sup> For example, several durability tests over  $>1000 \text{ h}$  of electrolyte-supported cell-based stacks have shown relative voltage increase rates as low as 0.5%–0.6%/kh.<sup>7,8,15</sup> While degradation rates of state-of-the-art stacks with fuel electrode supported cells seem to be higher on average,<sup>12,30–33</sup> some studies report degradation rates of 0.5%–0.7%/kh as well.<sup>10,11,13</sup> As a different metric, some long-term degradation studies prefer to use the resistance increase over time as a more accurate measure of degradation.<sup>7,8,12,14,15</sup> Here, values of  $12\text{--}18 \text{ m}\Omega \text{ cm}^2 \text{ kh}^{-1}$  were reported for state-of-the-art ESC stacks,<sup>6–8,12,15</sup> or  $20 \text{ m}\Omega \text{ cm}^2 \text{ kh}^{-1}$  for stacks with metal-supported cells were observed.<sup>14</sup>

At the same time, the oxygen side outlet temperature increased from 800 °C at the beginning to 802 °C after 1570 h and 805 °C after 4942 h due to the increased Joule heating inside the stack. Furthermore, the evolution of the gas-tightness of the stack was monitored by measuring the OCV in SOFC conditions, that is, with a dry fuel gas of 60% H<sub>2</sub> and 40% N<sub>2</sub>. Comparison of the OCV values between the beginning and the end of the stack lifetime showed a small decrease of some RUs of up to 36 mV for RU 2 which could have contributed to the increase in temperature over time to a small extent. However, the OCV of all RUs at the end of the test was above 1.19 V indicating a generally high gas-tightness of the stack.

For a more detailed analysis of the degradation behavior, impedance spectra at  $-0.39 \text{ A cm}^{-2}$  and  $-0.6 \text{ A cm}^{-2}$  and different times elapsed from the start of experiment were compared. Exemplary representative electrochemical impedance spectra of RU 6 are depicted in Fig. 8. In addition, the degradation rates for the ohmic, polarization and total resistance of all RUs at part load with  $-0.39 \text{ A cm}^{-2}$  are depicted in Fig. 9 and average values are

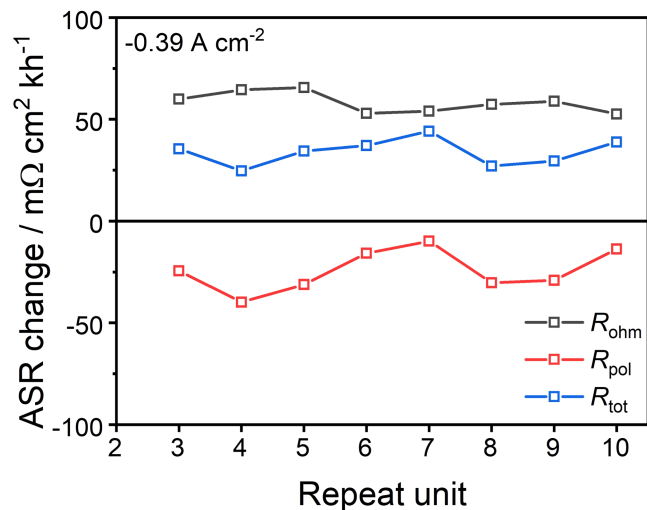


**Figure 9.** Calculated ohmic, polarization and total resistance degradation rates of all RUs derived from EIS measurements at the part load operating point with  $-0.39 \text{ A cm}^{-2}$ . A total normalization time of 3954 h was used which corresponds to the difference in time between the EIS measurements subtracted by the time at room temperature during the thermal cycles. No final impedances could be recorded for RU 1 and RU 2 due to measurement disturbances.

shown in Table II. All impedances showed an increase of the ohmic resistance over time which is commonly reported as the dominant degradation process for ESC. The average ohmic resistance degradation rate at part load was calculated to be  $58.2 \text{ m}\Omega \text{ cm}^2 \text{ kh}^{-1}$ , which corresponds to an average relative increase of ohmic losses by 68%. At  $-0.6 \text{ A cm}^{-2}$  the average ohmic resistance increased only by  $39.5 \text{ m}\Omega \text{ cm}^2 \text{ kh}^{-1}$ , which corresponds to a relative increase of only 45%.

Ohmic resistance increases of single cells are usually assumed to be predominantly caused by a gradual decrease of the ionic conductivity of the doped zirconia electrolyte.<sup>34,35</sup> Doped zirconia electrolytes have in some cases been reported to show a decrease in electrical conductivity of up to 30% in 3000 h.<sup>34,36</sup> Since the average ohmic resistance in the present study increased by 68%, it is likely that one or more additional processes significantly contribute to the ohmic resistance such as loss of contacting. For example, increased contact resistance on the air side was reported due to compositional changes of CuNiMn (CNM) oxide spinel contacts<sup>37</sup> and oxide scale formation on the interconnect.<sup>8</sup> Switching to the part load operating point at  $-0.39 \text{ A cm}^{-2}$  decreases the stack temperature considerably in comparison to operation at  $-0.6 \text{ A cm}^{-2}$  ( $T_4 = 766 \text{ }^\circ\text{C}$  vs  $789 \text{ }^\circ\text{C}$  at the end of the experiment) causing a change of the temperature-dependent conductivity values of all constituents according to an exponential law. The activation energy of the electronic conductivity in perovskites used for current collection ( $<0.6 \text{ eV}$ ) and the activation energy for electronic conductivity in  $\text{Cr}_2\text{O}_3$  on the interconnect (0.78 eV) are lower than the one for ionic conductivity in the 10Sc1CeSZ electrolyte (0.86 eV). The difference in activation energy barriers will lead to different contributions of the respective processes to the ohmic resistance at different current density/stack temperature. However, since the relative ohmic resistance change

over time decreases with current density and stack operating temperature, it is possible that some contact healing (re-contacting) at higher temperature takes place.

In contrast to the ohmic resistance, the polarization resistances showed a pronounced decrease over time mainly observed in the frequency region of  $\sim 10 \text{ Hz}$  (Fig. 6). This frequency range is most likely related to the LSMM'/ScSZ oxygen electrode, and the underlying reason for this activation effect remains unclear so far. The LSMM' used in the oxygen electrode is a strontium doped lanthanum manganite with an additional transition metal on the B site, and thus, has a similar structure as the  $\text{La}_{1-x}\text{Sr}_x\text{MnO}_{3-\delta}$  (LSM) perovskite which has historically frequently been used as SOFC cathode. However, its ionic and electronic conductivities are improved due to the B site doping.<sup>20</sup> The activation of LSM SOFC oxygen electrodes under cathodic polarization is a well-known phenomenon, and has suggested to be due to the removal of passivation SrO species from the surface and the formation of oxygen vacancies.<sup>38</sup> Hence, a similar mechanism could have occurred in the present work. The average polarization resistance decrease was determined to be  $-24.3 \text{ m}\Omega \text{ cm}^2 \text{ kh}^{-1}$ , which led to a partial compensation of the ohmic loss increase and an average total resistance degradation rate of  $33.8 \text{ m}\Omega \text{ cm}^2 \text{ kh}^{-1}$ .

The total ASR degradation rates for the different RUs at part load in Fig. 9 showed similar trends as the voltage changes in Fig. 7b with RUs 4, 8, and 9 showing the lowest degradation rates, and RU 7 the highest one. However, RU 9 showed an improvement of voltage over time and still a positive degradation rate. This counterintuitive behavior can be explained by the relation  $\Delta U = R(T, i) \Delta i$ , with the implication that the total resistance is not constant for the SOEL current density operating range, but a non-linear function of temperature and current density.

Large scattering in the low-frequency region hindered the calculation of degradation rates as exemplified by the impedance spectra at  $-0.6 \text{ A cm}^{-2}$  in Figs. 8c, 8d. Nevertheless, it can still be deduced that the overall resistance of RU 6 decreased at these operating conditions since its ohmic resistance increase was over-compensated by the decrease in polarization resistance which is in good agreement with the observed voltage behavior over time in Fig. 7a.

Thus, it is concluded that the stack showed outstanding performance stability over the investigated time period. However, the determined degradation rates were considerably impacted by an initially large increase of the ohmic resistance and a simultaneous decrease of the oxygen electrode resistance. The changes of both resistance contributions can be expected to level off over time and durability experiments with even longer testing times will be necessary to identify the stack technology's long-term stability in steady-state conditions.

## Summary and Conclusions

In the present study, the degradation behavior of a SOEL stack (type "MK35x") developed at Fraunhofer IKTS was investigated. An initial electrochemical characterization of the individual RUs of the 10-layer stack by means of EIS revealed in fuel cell and electrolysis operation different performance gradients over the height of the stack demonstrating the different temperature and gas flow distributions. A steady-state degradation test in steam electrolysis over more than 3000 h at the nominal full load operating point with a fuel inlet gas of

**Table II.** Average ohmic, polarization and total resistance of all RUs derived from EIS measurements at the part load operating point with  $-0.39 \text{ A cm}^{-2}$  depicted in Fig. 9 and the initial stack temperature  $T_4$ . A total normalization time of 3954 h was used which corresponds to the difference in time between the EIS measurements subtracted by the time at room temperature during the thermal cycles.

	$R_{\text{ohm}}$ [ $\text{m}\Omega \text{ cm}^2/\text{kh/RU}$ ]	$R_{\text{pol}}$ [ $\text{m}\Omega \text{ cm}^2/\text{kh/RU}$ ]	$R_{\text{tot}}$ [ $\text{m}\Omega \text{ cm}^2/\text{kh/RU}$ ]	Initial temperature in stack [ $^\circ\text{C}$ ]
$-0.6 \text{ A cm}^{-2}$	39.5	—	—	789
$-0.39 \text{ A cm}^{-2}$	58.2	-24.3	33.8	763




80% H<sub>2</sub>O, 20% H<sub>2</sub>, an oxygen side outlet temperature of 816 °C and a current density of  $-0.6 \text{ A cm}^{-2}$  corresponding to 82% SC showed a negative overall degradation rate (improvement) of  $-0.33\%/kh$ . By contrast, initial and final characterization at the part load operating point at  $-0.39 \text{ A cm}^{-2}$  and 800 °C oxygen side outlet temperature led to the determination of a positive overall degradation rate of  $0.4\%/kh$  showing a considerable impact of the operating conditions on the degradation rate. EIS measurements over time were demonstrated to be useful in unraveling the stack's degradation behavior and revealed an increase of the ohmic resistances and a decrease of the polarization resistances. The detailed analysis of electrochemical performance in SOEC and SOFC operation showed a severe increase of ohmic losses in most degraded cells. The decrease of the polarization resistance had its origin in the activation of the LSMM<sup>+</sup>-based oxygen electrode. The magnitude of these two effects changed between full and part load electrolysis operation and were the reason for the witnessed opposed trends in stack degradation behavior. The underlying mechanisms will be further investigated combining the obtained insights with results from destructive post-test analysis of the stack.

### Acknowledgments

The German Ministry of Education and Research (BMBF) is acknowledged for funding in the framework of the "SOC-Degradation 2.0" project under grant number 03SF0621B. We would like to thank the University of Bayreuth, Chair for Electrical Energy Systems, for providing the impedance analysis and modelling software ec-idea (<https://www.ees.uni-bayreuth.de/en/ec-idea>).

### ORCID

Matthias Riegraf  <https://orcid.org/0000-0002-0383-2545>

Michael Lang  <https://orcid.org/0000-0001-7756-9658>

Rémi Costa  <https://orcid.org/0000-0002-3534-1935>

### References

- Z. J. Schiffer and K. Manthiram, *Joule*, **1**, 10 (2017).
- M. Riegraf, R. Costa, and K. A. Friedrich, *Reference Module in Chemistry, Molecular Sciences and Chemical Engineering* (Elsevier, Amsterdam) (2024), in.
- Clean Hydrogen Joint Undertaking, *Strategic Research and Innovation, Agenda (2021–2027)*, <https://clean-hydrogen.europa.eu/system/files/2022-02/Clean%20Hydrogen%20JU%20SRIA%20-%20approved%20by%20GB%20-%20clean%20for%20publication%20%28ID%2013246486%29.pdf>, accessed on January 8, 2024.
- M. P. Hoerlein, M. Riegraf, R. Costa, G. Schiller, and K. A. Friedrich, *Electrochim. Acta*, **276**, 162 (2018).
- J. Schefold, A. Brisse, and H. Poepke, *Int. J. Hydrogen Energy*, **42**, 13415 (2017).
- C. Geipel, K. Hauptmeier, K. Herbrig, F. Mittmann, M. Münch, M. Pötschke, L. Reichel, T. Strohbach, T. Seidel, and A. Surrey, *ECS Trans.*, **91**, 123 (2019).
- M. Lang, S. Raab, M. S. Lemcke, C. Bohn, and M. Pysik, *Fuel Cells*, **20**, 690 (2020).
- S. Megel et al., *ECS Trans.*, **78**, 3089 (2017).
- M. Bertoldi, O. Bucheli, and A. Ravagni, *ECS Trans.*, **68**, 117 (2015).
- Q. Fang, L. Blum, and N. H. Menzler, *J. Electrochem. Soc.*, **162**, F907 (2015).
- G. Rinaldi, S. Diethelm, E. Oveisi, P. Burdet, J. Van Herle, D. Montinaro, Q. Fu, and A. Brisse, *Fuel Cells*, **17**, 541 (2017).
- J. Aicart, L. Tallobre, A. Surrey, B. Gervasoni, C. Geipel, H. Fontaine, S. Desousanobre, and J. Mougín, *Int. J. Hydrogen Energy*, **60**, 531 (2024).
- Q. Fang, C. E. Frey, N. H. Menzler, and L. Blum, *J. Electrochem. Soc.*, **165**, F38 (2018).
- P. Hjalmarsson, J. Harman, C. Macauley, I. Methley, J. Ryley, A. Zerfa, C. Hargrove, and M. Selby, *ECS Trans.*, **111**, 977 (2023).
- M. Riedel, M. P. Heddrich, and K. A. Friedrich, *Fuel Cells*, **20**, 592 (2020).
- M. Kusnezoff, M. Jahn, S. Megel, E. Reichelt, N. Trofimenko, G. Herz, W. Beckert, J. Schilm, A. Rost, and J. Schoene, *ECS Trans.*, **103**, 307 (2021).
- M. Kusnezoff, S. Megel, C. Rix, P. Adam, E. Reichelt, G. Herz, M. Jahn, N. Trofimenko, and A. Michaelis, *ECS Trans.*, **91**, 2579 (2019).
- C. Bienert, M. Brandner, S. Skrabs, A. Venskutonis, L. S. Sigl, S. Megel, W. Becker, N. Trofimenko, M. Kusnezoff, and A. Michaelis, *ECS Trans.*, **68**, 2159 (2015).
- S. Megel, C. Dosch, S. Rothe, M. Kusnezoff, N. Trofimenko, V. Sauchuk, A. Michaelis, C. Bienert, M. Brandner, and A. Venskutonis, *ECS Trans.*, **57**, 89 (2013).
- N. Trofimenko, M. Kusnezoff, and A. Michaelis, *ECS Trans.*, **35**, 315 (2011).
- S. Megel, M. Kusnezoff, N. Trofimenko, V. Sauchuk, A. Michaelis, A. Venskutonis, K. Rissbacher, W. Kraussler, M. Brandner, and C. Bienert, *ECS Trans.*, **35**, 269 (2011).
- N. Trofimenko, M. Kusnezoff, S. Mosch, and A. Michaelis, *ECS Trans.*, **91**, 263 (2019).
- M. Hahn, S. Schindler, L.-C. Triebs, and M. A. Danzer, *Batteries*, **5**, 43 (2019).
- M. Lang, C. Auer, G. Braniek, F. Wenz, and F. Hauler, *ECS Trans.*, **68**, 2441 (2015).
- M. Riegraf, M. P. Hoerlein, R. Costa, G. Schiller, and K. A. Friedrich, *ACS Catal.*, **7**, 7760 (2017).
- M. Riegraf, R. Costa, G. Schiller, K. A. Friedrich, S. Dierickx, and A. Weber, *J. Electrochem. Soc.*, **166**, F865 (2019).
- C. Grosselindemann, N. Russner, S. Dierickx, F. Wankmüller, and A. Weber, *J. Electrochem. Soc.*, **168**, 124506 (2021).
- M. Riegraf, F. Han, N. Sata, and R. Costa, *ACS Appl. Mater. Interfaces*, **13**, 37239 (2021).
- W. G. Bessler and S. Gewies, *J. Electrochem. Soc.*, **154**, B548 (2007).
- D. Schäfer, Q. Fang, L. Blum, and D. Stolten, *J. Power Sources*, **433**, 126666 (2019).
- G. Corre and A. Brisse, *ECS Trans.*, **68**, 3481 (2015).
- J. Aicart, A. Surrey, L. Champelovier, K. Henault, C. Geipel, O. Posdziech, and J. Mougín, *Fuel Cells*, **23**, 463 (2023).
- J. Mougín, A. Chatroux, K. Couturier, M. Petitjean, M. Reytiér, G. Gousseau, and F. Lefebvre-Joud, *Energy Procedia*, **29**, 445 (2012).
- J. Kondoh, T. Kawashima, S. Kikuchi, Y. Tomii, and Y. Ito, *J. Electrochem. Soc.*, **145**, 1527 (1998).
- F. T. Ciacchi and S. P.-S. Badwal, *J. Eur. Ceram. Soc.*, **7**, 197 (1991).
- M. R. Termer, J. A. Schuler, A. Mai, and D. Penner, *Solid State Ionics*, **263**, 180 (2014).
- M. Brandner, C. Bienert, S. Megel, M. Kusnezoff, N. Trofimenko, V. Sauchuk, A. Venskutonis, W. Kraussler, A. Michaelis, and L. S. Sigl, *ECS Trans.*, **57**, 2235 (2013).
- S. P. Jiang, *J. Mater. Sci.*, **43**, 6799 (2008).